

Response to Reviewer RC1

General Remarks

Thank you for the supporting review. The minor corrections are mentioned below

Detailed Response:

p.1, line 30: no hyphen in debris flow

Modified

p. 2, line 55: avoid repetition of vary. Maybe use "...different surges can vary...."

Modified

p. 15, line 272: insert "laterally" before "deposit"

Modified

p. 16, line 77: write "debris-flow front", with hyphen and -r

Modified

p. 17, line 279: write "debris-flow LSPIV velocity...", include mean/average to the figure caption and add a value of the temporal rate/point density of the red, yellow and blue line

modified

p. 18, line290: there seems to be missing something in this sentence. Please check

It seems complete, without any lengthy wording.

p. 19, line 299: reformulate the sentence. Maybe start with "We suspect, we hypothesize..."

Modified to "We suspect"

debris flow with hyphen when used as adjective, e.g. p. 21, lines 341, 355 or p. 22, lines 359 and 360

Modified

It is not described well enough how much the effort is and how good the foundations must be for the accuracy to be achieved.

Mean differences with the radar sensors are restated in the conclusions. It is difficult to say how much effort is required to get these accuracies, we provide a field example, more study sites are needed to provide better guidelines.

Citations: Please add the new paper by Jacquemart et al. to your introduction. Maybe just add "...the application of LSPIV from video images on debris flows..." to p.2, line 60.

Citation is added

Response to Reviewer RC2

General Remarks

Thank you for the detailed review. There have been key insights, particularly the turbulence analysis that have helped improve the article. Both flow direction variation and velocity variation are now used in the turbulence analysis. Improvements have been made in the methods description, figures, and interpretation of results as the reviewer has proposed.

Detailed Response:

I. 59: (Stumpf et al., 2017) > 2016, Please carefully check all references.

Modified

I. 79 : "began in 2011, refer to Comiti et al. (2014)"

I feel something is missing in this sentence. Maybe . . ."AND WE refer to. . ."

Clarified to "for detailed information of the study site and monitoring setup, refer to Comiti et al. (2014)"

I. 81: "Two cameras are in a sediment trap. . ." Certainly they are not really IN the sediment trap but maybe rather ALONGSIDE?

Modified

I. 87-91: Providing specific number on the incidence angles and distances which worked/ did not work might help others to set up networks which are suitable for LSPIV. From this explanation is also seems that the network was initially not setup with LSPIV in mind. Please clarify. I'd also change ", coupled to" to "in combination with". A first look on Fig. 3 also suggests that the image quality from the two other cameras is reasonable and some further explanation would help the readers to understand why the videos could not be exploited.

This section is now clarified with incidence angle range. Distances are not so useful and can be misleading since it depends on camera resolution, and if the reader is interested, it can easily be estimated in Figure 1. It is also clarified that the other two cameras were in fact too close, limiting the area for the scale of a debris flow.

Figure 1: Why is a part of the analyzed cross-section behind the camera 2? Maybe this is an error in the Figure? Even if the fish eye lens covers a wide panoramic view it will probably not cover objects which are more than 90° of the image center?

The camera symbol was not appropriately angled, it is now repositioned in the figure.

I. 101: "based from Le Boursicaud" > based ON Please carefully check the use of English language in the manuscript and consult a native English speaker if possible.

Grammatical overlook was corrected

3.1 Video treatment: I feel that at some point you should provide more details about the camera system such as focal length, resolution, lens type, options for night time observations (did you test such options?), color vs greyscale, etc.

Camera model and resolution are added. There were no events during the night. Spotlights are triggered during rainfall in the night.

I. 107: “initially posed as a problem” > initially posed problems

Modified to “initially was a problem”

I.108: “During recording of the flow events, the frequency reduced to 2-3 fps because of the low lighting of the storms. . . .therefore we subsampled the images to the minimum frame rate of each flow event”

Could you please explain why exactly the frame-rate is reduced? Changes in the illumination conditions can be compensated with changes in the ISO or the aperture, rather than by the shutter speed. Does a lower shutter speed not lead to blurry images for something moving as fast as a debris flow? In addition, to avoid subsampling, you could just use the time-stamps of each frame, which can be extracted with tools such as FFMPEG. Did you check that the nominal frame rate corresponds exactly with the time-stamps of individual frames? There can be bad surprises where the actual frame rate varies even if the nominal frame-rate is set constant.

The IP camera that we used had limited features (now added to the article). No automatic ISO and aperture settings.

For the subsampling, the camera copies previous frames to fill in the holes of the adjusted frame rate. We took special care that the frame rates were correct with the subsampling and validating with the time-stamps. I believe that these are confusing little details that can ruin the flow of the article.

I. 111 ff.: Could you provide an estimate of the accuracy of the lens calibration? Since, you are already explaining the camera calibration; it would also seem logical to indicate here how you determined the camera orientation.

The camera orientation is not required for orthorectifying images, just an undistorted image with enough reference points (done manually in Hugin). The accuracy of the undistortion was not recorded, it is not very relevant since the images will be rectified with reference points afterwards.

I. 123: “resolution colored point clouds (1300-2900pts/m3) making it a reliable spatial and visual reference. For the LSPIV purposes, the point clouds were rotated to make a horizontal flow plane.”

The point density is not a good indicator for the quality of the surface reconstruction. Could you provide an independent measurement to estimate the accuracy of the derived point clouds? How did you georeferenced the point cloud? It is not clear why the rotation is needed and how you assured that the ‘flow plane’ is indeed horizontal after the rotation. The channel certainly has a significant slope, though isn’t it an error to assume that it is horizontal? Please clarify.

The ultra-high resolution of colored points is relevant for visually matching the reference points to the images. However, yes, it should include an error, the alignment error from ICP calculations are included.

The 5.7 degree rotation (approximate channel slope) is indicated. Some clarification is added mentioning it is to reduce any added spatial error.

I. 130-135: This paragraph needs further clarification. 1. What exactly is the purpose of matching the point clouds and the video imagery (determining camera orientation?) 2. You state that “Errors increase going down and across the channel according to the camera’s oblique angle.” Errors of what? How did you quantify them and what is there magnitude? 3. You state that “The flow plane elevation was also measured by averaging matched features touching the flow line in the post-event point cloud.” So the underlying assumption is that the flow height is locally constant (i.e. a horizontal plane)? How realistic is this assumption or on other words how steep is the channel? How does this relate to rotation to the point cloud mentioned earlier? Given that you undertake multiple measurements; could you provide an uncertainty of the plane elevations? 4. You might also want to explain briefly the rectification process in which the video frames are projected to the plane(s) since not all readers of NHESS might be sufficiently familiar with LSPIV processing.

1. To clarify further the paragraph, it now begins with “For orthorectifying video images...”

2. It is the alignment error for orthorectification. Errors are indicated in Table 1. This is now clarified in the text.

3. Variable rough flow height is added... the flow height is the best estimate. There are not enough measured points to make an uncertainty (approximately 5-10 measurements).

4. The rectification is standard georeferencing methods such as in GIS. LSPIV process is described in the next paragraphs.

I. 140: “(3.75 -5 m) downstream, 60 -100 pixel (3-5 m) wide, and a small 5 pixel segment upstream to capture any perpendicular flow”

What do you mean by perpendicular flow here? Please clarify.

Changed to “...capture flow directions toward the banks.”

I. 150: “horizontal turbulence index (T_h). We measure T_h by taking the standard deviation of the flow directions at a given cross-section for a given surge”

This is fairly simplistic indicator compared to a real decomposition in mean and turbulent flow commonly used in fluid mechanics. Its shortcomings (e.g. fluctuations in speed are ignored) should at least be acknowledged. A formula for T_h should be provided since computing the standard deviation of a circular quantity requires some transformations.

It is a simplistic indicator, it is easier for the reader to read the explanation rather than the equation, further clarified “Standard deviation of vector orientations in 3 adjacent cross-sections for three time-steps.”

Fluctuation in speed analysis (T_v) is added in the methods and analysis, with the same turbulence calculation (just with vector velocity rather than direction). T_h is now T_d

3.4 Visual velocity reconstruction

The use of Cam1 and Cam3 for carrying out manual reference measurements implies that the internal and external parameters for those cameras have been calibrated. Please clarify if you used the same procedure described above for all cameras. Are the “Visual” values in Table 2 derived from Cam1 and Cam3? Given the numerous points that can be measured both automatically and manually it seems odd to provide only a single value for each section in the debris flow in Table 2. A mean and a standard deviation for both LSPIV and visual measurements would be much more meaningful.

There had been hesitation in including this section, reviewers confirm our hesitation. It is now omitted

5.1 Surface flow velocities

- “Mean surge velocities” . . . Please explain earlier how the means are computed - H_t or T_h ? - The velocities given in Figure 4 do not fully match with what is reported in Table 2. Assuming that the crosses mark the distribution mean (which should be indicated in the figure caption) it seems that for example that for 2013 S1 inter and S1 tail are marked at around 3.0 and 2.0 while in Table 2 values of 2.5 and 2.7 are provided respectively. Please ensure that your results are correct and consistent (also in Fig 5). - For the interpretation of Figure 4 it would also be helpful to use the time on the X-axis and place the boxplots accordingly for each event. Presenting the cumulative rainfall pattern along with this may then also help to better clarify and interpret the events. - “. . .the feature picking does not always represent the flow velocity accurately. . .” I agree. Feature picking is typical less precise and comprises the same systematic errors resulting from camera calibration and rectification. I might be helpful to recall this here.

The data in the table were mistakenly the mean velocities for the LSPIV area (not within the cross-section). The correlations coefficients have decreased but trend lines have changed by a little in Figure 10. However, they are still important. The mean differences with velocities from the radar have improved in Figure 5.

Furthermore, the new T_v (Turbulence from velocity variation) has a much better correlation than the T_d .

T_v results with also be included in Figure 4 and Figure 10 and included in the discussion.

There are multiple source areas and the rainfall data opens a door to much more analysis with sediment dynamics in the catchment, it is kept for a future article.

For Figure 4, the surge labels are easier to read, rather than the long written time periods.

Regarding Figure 6:

- Where is the dam you are referring to? Maybe indicate it in Fig 1.

- The dashed blue line (left figure) is strange and could give the impression that the flow suddenly stops after a strong acceleration. Please explain.

- Maybe indicate on the left figure which section was observed with which camera.

- The figure on the right is a bit messy. It is nearly impossible to clearly associate all trend lines with their respective points. Why do some series have trend lines while others do not?

- Given the complexity debris flows (different rheologies, kinetic energy, etc.) plus the presence of check dams (Figure 1) and changes in the channel width make it seem elusive to establish a simple relationship between velocity and slope. I would recommend adapting this section either by increasing the complexity of the interpretation or omitting the analysis.

There had been hesitation in omitting this section, reviewers confirm our hesitation. It is now omitted

I. 245: “of the average velocities for the front, intermediate and tail” For the interpretation it would be helpful to recall here the time intervals for each average.

Time periods are now included

Figure 7: The background images are hard to interpret for readers not familiar with the site. Maybe add some further information such as the outline of the debris flow in each image to facilitate the interpretation.

Better rectified photos are added that highlight the flow better

I. 250 ff: Regarding Fig. 8 I'm a bit surprised regarding the spikiness of the time-series (even after averaging along the profile). Do you consider this a plausible feature of the debris flow or could this be a residual of the LSPIV method.

This is most likely some residual turbulence in the profile and heterogeneity of the flow.

Figure 8: Please improve the legend and caption of the figure on the left side. What you show here seems rather a difference between two dates rather than a residual. Furthermore, please explain why the time-series is interrupted around 17:23:34.

The figure is improved with a better legend and captions.

The time-interruption was initially made to make a clear distinction between the front and the rest of the flow.

This was a period of channel adjustment during the boulder front deposition

Figure 9 also requires further improvements. Please enumerate the subfigures according to the journal guidelines and provide separate captions for each of them. Maybe indicate in Figure 8 where the profile in Figure 9 starts.

Sub-figures are enumerated and captions added. The grid is added to Figure 9 for easier referencing to Figure 8.

I. 305: For the sake of completeness g should be defined.

Not relevant anymore

I. "We propose that the Th measurement improves the flow resistance coefficient for estimating velocity." This seems a bit curious since you measure velocity directly with LSPIV. Would it not be more useful to use Th as an alternative to estimate rheological parameters which are typically harder to derive? Please clarify.

The rheological parameters can be measured in the field without video monitoring events. It is very useful for improving these estimates for modeling purposes.

Exploiting LSPIV to assess debris flow velocities in the field

Joshua I. Theule^{1,3}, Stefano Crema², Lorenzo Marchi², Marco Cavalli², Francesco Comiti¹

¹Faculty of Science and Technology, Free University of Bozen-Bolzano, Bozen-Bolzano, 39100, Italy
²Research Institute for Geo-hydrological Protection, National Research Council of Italy, Padova, 35127, Italy
³TerrAlp Consulting, 100 chemin du grand pré, 38410 St Martin d'Uriage, France
Correspondence to: Joshua I. Theule (joshua.theule@terralpconsulting.com)

Abstract. The assessment of flow velocity has a central role in quantitative analysis of debris flows, both for the characterization of the phenomenology of these processes, and for the assessment of related hazards. Large scale particle image velocimetry (LSPIV) can contribute to the assessment of surface velocity of debris flows, provided that the specific features of these processes (e.g. fast stage variations and particles up to boulder size on the flow surface) are taken into account. Three debris flow events, each of them consisting of several surges featuring different sediment concentration, flow stage and velocity, have been analyzed at the inlet of a sediment trap in a stream of the eastern Italian Alps (Gadria Creek). Free softwares have been employed for preliminary treatment (ortho-rectification and format conversion) of video-recorded images as well as for LSPIV application. Results show that LSPIV velocities are consistent with manual measurements on the ortho-rectified imagery and with front velocity measured from the hydrographs in a channel reach approximately 70 m upstream of the sediment trap. Horizontal turbulence, computed as the standard deviation of the flow directions at a given cross-section for a given surge, proved to be correlated with surface velocity and with visually estimated sediment concentration. The study demonstrates the effectiveness of LSPIV in the assessment of surface velocity of debris flows, and permit to identify the most crucial aspects for improving the accuracy of debris flows velocity measurements.

1 Introduction

Debris flows are a rapid flow of saturated non-plastic debris in a steep channel (Hungr et al., 2001). They consist of poorly sorted sediments mixed with water and organic debris with sediment concentrations higher than 50% by volume or 70% by mass (Costa, 1984; Phillips and Davies, 1991) and can travel over long distances at relatively high velocities (generally between 2 to 20 m s⁻¹) (Iverson, 1997; Rickenmann, 1999). Debris flows are relatively infrequent and complex events which make it difficult to characterize their dynamic flow heights, velocities, discharge, and flow resistance of the material, among other aspects. Debris-flow velocities and discharge are typically backcalculated from surveyed channel bends with superelevated flow heights using the forced vortex equation (eg. Hungr et al., 1984; Chen, 1987; Prochaska et al., 2008; Scheidl et al., 2014). The measured parameters (flow heights, velocity, and slope) from post-event surveys for this equation can also be used to estimate flow resistance coefficients to understand the viscosity and sediment concentrations of the debris flows (eg. Rickenmann, 1999). However, sediment concentrations are known to significantly increase and decrease during the

Formatted: Italian (Italy)

Deleted: -

33 propagation of the flow (eg. Pierson and Scott, 1985; Rickenmann et al., 2003) and the velocity profile of the surges can also
34 vary thus limiting the reliability of post-event field methods.

35 Debris-flow monitoring projects are growing thanks to the increasing feasibility and capability of observing several
36 parameters of this complex process (eg. Marchi et al., 2002; Coe et al., 2008; Arattano et al., 2012; Navratil et al., 2013;
37 Comiti et al., 2014). Typical monitoring stations consist of geophones, ultrasonic sensors (or radar), and video cameras
38 which satisfy the basic measurements of velocity, height, discharge, and visual validation. Some catchments present also
39 multiple stations distributed throughout the debris-flow channel and some located in headwater channels (Berti et al., 2000;
40 Marchi et al., 2002; Hürlimann et al., 2003; McCoy et al., 2010; Arattano et al., 2012; Navratil et al., 2013; Comiti et al.,
41 2014).

42 Video acquisitions originally started as a validation of the instrumented recordings and visual interpretation, but as cameras,
43 power, and storage capacities improve, further analysis can be made. Manual tracking of particles with field measurements
44 can measure velocities accurately when compared to stage sensors (eg. Arattano and Grattoni, 2000; Marchi et al., 2002).
45 The video imagery of debris flow can also be used to interpret the turbulence, sediment mixture, sediment concentration,
46 presence of rigid plugs and laminar flows (eg. Marchi et al., 2002). Horizontal velocity distributions from video imagery
47 have shown variations of flow resistance between events and within the same surge (Genevois et al., 2001). Rheological
48 parameters are known to significantly vary within the same surge, but they are very difficult to quantify in the field.

49 Large scale particle image velocimetry (LSPIV) is another video imagery technique often used in rivers to measure two
50 dimensional velocities from high resolution images at high frame rates (eg. Fujita et al., 1998; Hauet et al., 2008; Le Coz et
51 al., 2010; Muste et al., 2014). Cross-correlations are made between time-step imagery within a given search window. This is
52 typically applied in steady flows by tracking bubbles, ice, debris, and artificial seeding. Discharge rates can then be
53 estimated because of the stable cross-sections during the flow. LSPIV and series of elevation models were also compared
54 during bedload transport flume experiments to quantify discharge and deposition, as well as Froude and Shield's numbers.

55 These types of analysis are difficult for debris flows because the different surges can vary in height and significantly modify
56 the channel bed. The LSPIV method was tested on a pulsing flash flood in a stable reach from a GoPro recording that was
57 available on Youtube (Le Boursicaud et al., 2016). There was a 3-5% velocity error for 15-30 cm water level bias which was
58 the largest source of error in the analysis. Recently, a long-term discharge monitoring project of a mountain stream with
59 LSPIV applications used an automated detection of the water level heights (Stumpf et al., 2016). This method still poses a
60 problem for the highly irregular debris-flow surfaces, however considering the low percent error, approximate heights should
61 be feasible for surface velocity. Laser profile scanners were also used in LSPIV applications for measuring debris-flow
62 velocities with direct comparisons of flow heights providing accurate discharge measurements and analysis of the flow
63 dynamics (Jacquemart et al., 2017).

64 To our knowledge, the application of LSPIV on debris flows from video images has not been deeply investigated whereas it
65 could provide direct measurement to quantify rheological behavior of debris flows. Our objective is to test the LSPIV
66 method on debris flows using available cameras in a monitored catchment in the Italian Alps (Gadria catchment) (Fig. 1).

- Deleted: which limit
- Deleted: High-frequency monitoring
- Deleted: Monitoring projects of debris flows
- Deleted: because of their
- Deleted: for
- Formatted: Italian (Italy)
- Deleted: even have
- Deleted: imagery
- Deleted: (Piton, 2016).
- Deleted: varying
- Deleted: 7
- Deleted: monitoring
- Deleted:

79 The aims of this work are to explore: 1) the spatial and temporal variation within one study reach of debris-flow surges
80 occurred in the period 2013-2015, 2) a detailed analysis of an individual surge dynamic, 3) the quantification of a “horizontal
81 turbulence index” (influenced by rheological parameters) from the directional variation of vectors, and 4) the
82 limitations/perspectives of the LSPIV for further development.

83 **2 Setting**

84 The Gadoria catchment is situated in Vinschgau-Venosta Valley (South Tyrol) in the Eastern Italian Alps (Fig. 1A), and
85 features a drainage area of 6.3 km² (between 1394 and 2945 m a.s.l.), with an average slope of 79.1 %. The source area
86 consists of highly deformed and fractured metamorphic rock, thick glacio-fluvial deposits and steep topography which
87 makes the catchment prone to rockfall, landslides, avalanches and debris flows. The topographic settings of the catchment
88 ensure an effective connectivity of sediment between the source areas (D’Agostino and Bertoldi, 2014) and the downstream
89 channel reaches (Cavalli et al., 2013). Debris flows occur in the summer and are usually triggered by spatially-limited
90 convective storms. The mean volume of the debris flows observed between 1979 and 2013 is 14,000 m³ (median 8000 m³)
91 (Aigner et al., 2015). The sediment yield of the Gadoria catchment between 2005 and 2011, a period normal as to frequency
92 and magnitude of debris flows, was computed through DEM differencing (Cavalli et al., 2017) and amounted to about 5200
93 m³km⁻²yr⁻¹. Instrumented monitoring of the Gadoria catchment began in 2011, for detailed information of the study site and
94 monitoring setup, refer to Comiti et al. (2014).

95 Two cameras are alongside a sediment trap (retention basin) near the alluvial fan apex, one looking upstream (Cam1) and the
96 other looking down at a more perpendicular angle to the flow (Cam2). The third camera (Cam3) is in the next reach
97 upstream from the sediment trap at a closer proximity to the flow (Fig. 2). These three cameras are connected to a cabin
98 equipped with power supply and a server (8 Tb storage capacity) collecting all the monitoring data. The fourth camera is in
99 an upstream ravine and it is triggered by a rain gauge when there is at least one minute of rainfall. For this study, we focused
100 on the application of LSPIV using only one of the four MOBOTIX M12 video cameras, Cam 2.

101 We attempted to utilize the other cameras for LSPIV application, but Cam 1 and Cam 3 were too close with an upstream
102 view to measure the large scale of the debris flow. Within the area of high incidence angle of the images, the number of
103 reference points is restricted, there is little spatial coverage, and there was too much pooling of water in front of Cam 1
104 located at the dam. Cam 2 was the best option because it was located higher on top of the levee (10 - 52% incidence angle),
105 12 - 46 m from the LSPIV area, and had an orientation more perpendicular to the flow path. Cam 4 was problematic due to
106 the unchannelized nature of the recorded events, in combination with the relative long distance between the camera and the
107 moving sediment.

Deleted: (between 1394 and 2945 m a.s.l.)
Formatted: Do not check spelling or grammar

Deleted: 6

Deleted: for detailed information of the study site and monitoring setup
Deleted: in

Deleted: also
Deleted: low

Deleted: , and this creates very skewed images with little ground coverage for LSPIV
Deleted: with
Deleted: angle
Deleted: coupled
Deleted: to

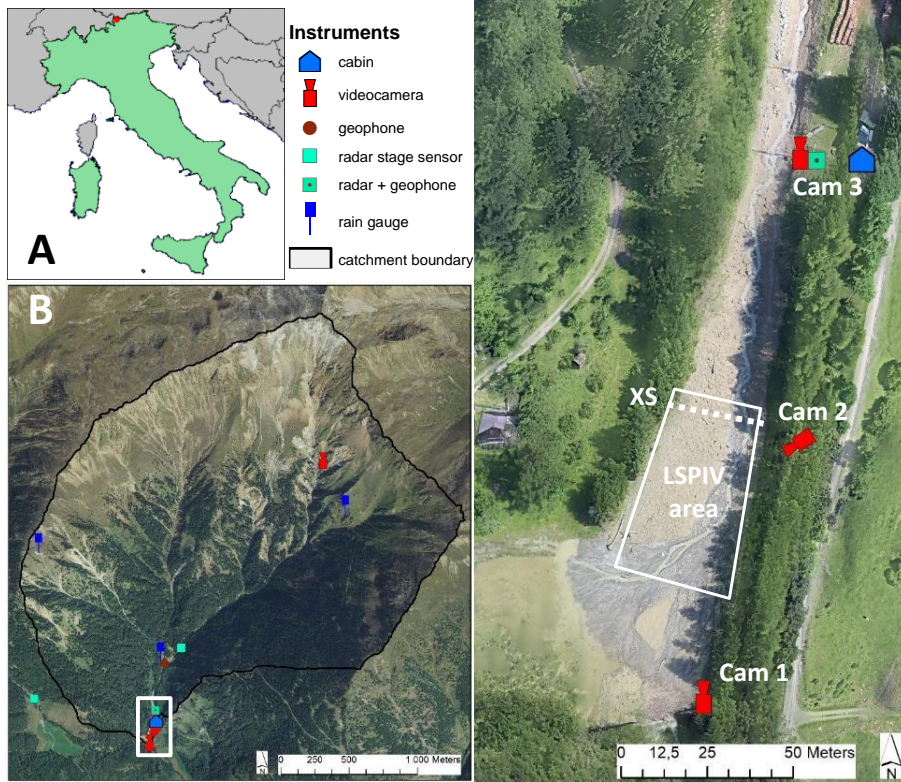


Figure 1: Gatria catchment is situated in the Vinschgau-Venosta Valley, South Tyrol, Italian Alps (A, red dot). The catchment is instrumented with rain gauges, radar stage sensors, video cameras, and geophones (B). At the end of the catchment (C) is a sediment retention basin where most of the instrumentation exists: XS: cross sections used in LSPIV measurements.

Deleted: connected to a cabin with a power supply, internet connection, and a server with 8 Tb of storage capacity.

130 **3 Methods**

131 The LSPIV methods that we used are based on Le Boursicaud et al. (2016). The previous study tested the LSPIV method on
132 a pulsating flashflood in the French Alps recorded from a GoPro. The videos were treated for photo stitching and format
133 conversion using freeware and the LSPIV calculation on the freeware Fudaa-LSPIV (Le Coz et al., 2014)
134 (<https://forge.irstea.fr/projects/fudaa-lspiv/files>).

135 **3.1 Video treatment**

136 The M12 Mobotix security camera that we used is an IP camera (resolution 1689x1345) with a fish eye lens, during the night
137 spotlights are activated during rainfall. This camera has limiting features such as an automatic adjustment for shutter speed
138 with illumination, and therefore the frame per second cannot be fixed. This initially was a problem since our aim was to have
139 a constant 10 frame per seconds (fps). During recording of the flow events, the frequency reduced to 2 - 3 fps because of the
140 low lighting of the storms. We needed a standard frame rate for LSPIV calculations, therefore we subsampled the images to
141 the minimum frame rate of each flow event (Table 1).

142 Also, since the camera had a fisheye lens, significant distortion correction was required. A checkerboard pattern image from
143 the camera was used in a free software Hugin (<http://hugin.sourceforge.net>) which has a tool for distortion correction. This
144 was then applied to all the video imagery and converted to an ASCII grey scale format using batch processing in the XNview
145 freeware (www.xnview.com). This used to be necessary for the Fudaa software, however it now can handle jpeg and tiff
146 colored formats.

147 **3.2 Reference points using Structure from Motion Photogrammetry**

148 High-resolution colored point clouds from Structure from Motion (SfM) surveys were found to be very useful for matching
149 reference points with the video images (Fig. 2A). In active debris-flow channels, permanent points are difficult to keep
150 within the active area, and with oblique angled cameras, there needs to be as many reference points as possible. The
151 sediment trap and channel were surveyed before and after flow events by walking up and down the banks with a camera
152 mounted on a 5-m pole with georeferenced targets (measured by total station) distributed throughout the channel and trap.
153 The SfM photogrammetry using AgiSoft® Photoscan (eg. Westoby et al. 2012; Javernick et al., 2014; Piermattei et al. 2015)
154 was used to generate high resolution colored point clouds (1300-2900 pts/m³) with 2 cm alignment error (using an iterative
155 closest point algorithm on permanent features), making it a reliable spatial and visual reference. For the LSPIV purposes, the
156 point clouds were rotated to make an approximate horizontal flow plane (5-degree rotation) to reduce any added spatial error.
157 These flow planes are easily visible in the colored point clouds with distinct mudlines.

Deleted: initially

Deleted: from

Deleted: and they are automatically adjusted to the available light

Deleted: posed as

Deleted: therefore

Deleted:

Deleted:

Deleted:)

Deleted: the

Deleted: .

170 Table 1: LSPIV parameters used for the 2013, 2014, 2015 events.

| | 2013 | 2014 | 2015 |
|-------------------------------------|--|--------|---------|
| resolution | 5cm/pixel | | |
| alignment error near the flow plane | 3-10 cm | 4-7 cm | 8-13 cm |
| # reference points | 13 | 13 | 14 |
| interrogation area | 26 pixel (1.3 m) | | |
| search area (pixels) | 75-100 down; 5 up; 35-50 left; 30-50 right | | |
| time step | 0.333 s | 0.5 s | 0.5 s |
| grid | 0.4-1.2 m | | |
| area | 28-35 m long and 7-32 m wide | | |

171 3.3 Fudaa LSPIV

172 For orthorectifying the video images, targets and natural features were used as reference points for matching between the
173 SfM point cloud (both pre-event and post-event) and video imagery (Fig. 2A, 2B). Corners of rocks next to the flow line
174 were typically used on each side of the channel, and sometimes exposed stable rocks within the channel. Alignment errors of
175 the reference points (Table 1) in the orthorectification process of Fudaa-LSPIV increase going down and across the channel
176 according to the camera’s oblique angle. The flow plane elevation was also measured by averaging matched features
177 touching the flow line in the post-event point cloud, this is the best estimate for the rough variable surface of the flow height.
178 The unsteady flows also required separating the fronts and tails to redefine the flow plane elevation which is known to be the
179 largest source of error for LSPIV (Le Boursicaud et al., 2016).

180 The interrogation area (IA) is the boundary for calculating a correlation coefficient which needs to be representative of the
181 flow velocity (Fig. 2C). It should find the travel distance of general features in the flow between each time step, not
182 individual particles, which is unrealistic in irregular flows with sediment rolling and continuously being submerged. We used
183 a 26 x 26 pixel (1.3 m x 1.3 m) interrogation area for calculating the correlation coefficient and a search area of 75-100 pixel
184 (3.75 - 5 m) downstream, 60 - 100 pixel (3 - 5 m) wide, and a small 5 pixel segment upstream to capture flow towards the
185 banks.

186 To have a good spatial distribution of the flow with a manageable dataset, we selected a grid with an approximate spacing of
187 0.7 m (varies with flow width) (Fig. 2C). Within the Fudaa software, we filtered any velocities with a correlation coefficient
188 less than 0.5-0.6 for a robust dataset (Fig. 2D). The velocity vectors were transferred into ArcGIS and overlaid on the
189 corresponding orthorectified image for manual cleaning. Noisy data can occur outside of the flow area because of rain, wind,
190 changing light reflection on wetted surfaces. The manual treatment of the vectors was also necessary for outlining and
191 separating the different surges and parts of the surge (front and tail) traveling through the study reach.

192 The spatial distribution of velocity vectors covering the reach provided an opportunity to examine their variation (direction
193 and velocity fluctuation) to characterize the turbulence of the various debris-flow surges (Costa 1984). Since our LSPIV
194 method is in the two dimensions, we define it as the horizontal turbulence index according to directional variation (T_d) and
195 velocity variation (T_v). We measure the turbulence (T_d and T_v) by taking the standard deviation of vector orientations (T_d) and

Deleted:

Deleted: any perpendicular flow

Deleted: the

Deleted: of directional variation of the velocity vectors

200 ~~velocities (T_v) in 3 adjacent cross-sections for three time-steps.~~ The given ~~segment of~~ cross-sections can be used to examine
201 the changing characteristics of the surges rather than the spatial ~~distribution~~. Therefore, small T_v and T_d should represent
202 laminar flows and ~~higher values are~~ more turbulent flows.▼
203 The LSPIV results were taken from cross-section XS (Fig. 1C) to have accurate comparisons of debris flow surges. This is
204 the most stable cross-section before the widening in the sediment trap. It is also the closest and most perpendicular view
205 from the camera resulting in the most accurate LSPIV calculations. The LSPIV study reach experienced important
206 deposition and remobilization during the debris flow surges, therefore we did not attempt to measure the discharge rates.

207 ▼

Deleted: standard deviation of the flow directions at a given cross-section for a given surge

Deleted: variation

Deleted:

Deleted: 3.4 Visual velocity reconstruction¶
Even though Cam 1 and Cam 3 could not be used for LSPIV, they were useful for tracking the surge fronts passing over check dams and boulders for approximately 250 m. Some of these velocities directly covered the reach upstream from the trap where the stage sensors were located for useful velocity comparisons. The spatial distribution of front velocities could also be examined given the changing of slope from the reach to the trap. Even though the stage sensors are approximately 70 m upstream from the LSPIV area, it still gives an approximate verification of velocities.¶

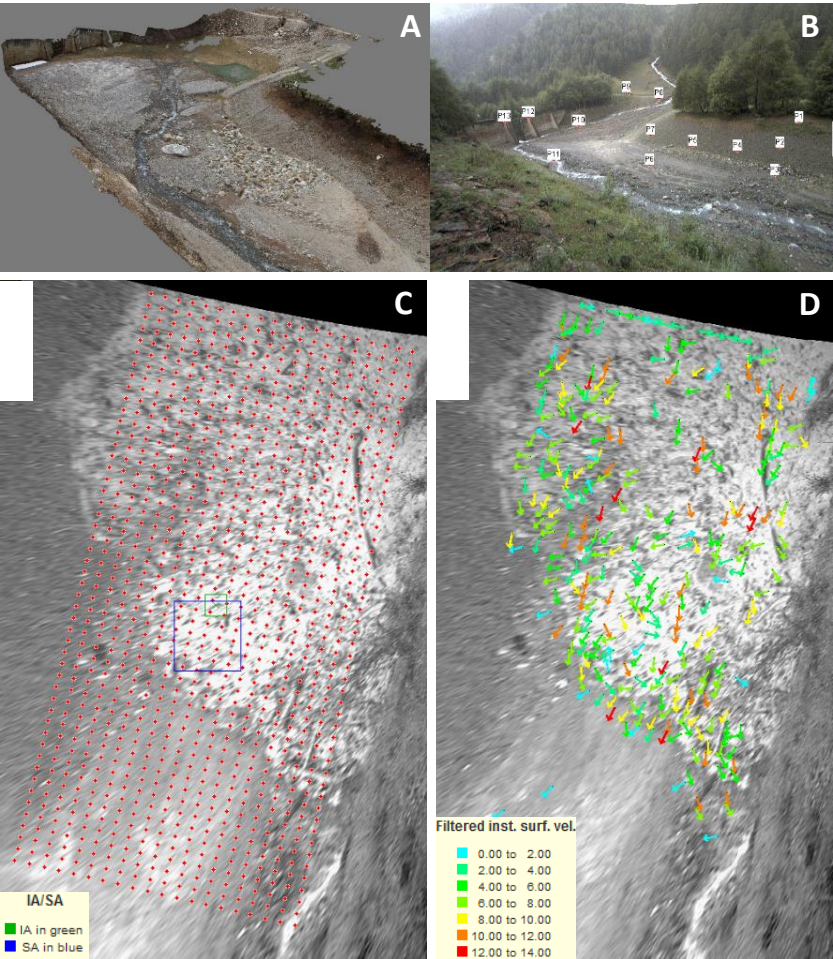


Figure 2: Example of (A) a SfM point cloud used as a post-event reference, (B) the undistorted camera image with the reference points, (C) the orthorectified image during the 2013 debris-flow front with the sampling grid, interrogation area (IA) and the search area (SA), and (D) the instantaneous surface velocity vectors.

227 **4 Analysed events**

228 [In the 2011-2015 time span](#), there have been four important events (Table 2; Fig. 3). The 2011 event was complex, with the
229 first and most important surge consisting of a hyperconcentrated flow and, only Cam 1 and Cam 3 were operational at the
230 time (Fig. 3). Therefore, LSPIV was not performed; measurements of flow velocity were performed manually (ratio of the
231 time interval between the passage of the front and the distance between the two radar sensors) and by means of cross-
232 correlation between the stage recordings (Comiti et al., 2014). There were no significant events in 2012.

233 The 2013 event featured one important surge, very typical debris-flow formation with a boulder front and the slurry-like tail.
234 The singular surge provided a convenient detailed analysis of the front, intermediate stage (transition from front to tail), and
235 the tail (described later).

236 The 2014 event had a small preliminary surge (pre-surge) and four debris flow surges passing through the study reach. It
237 should be noted that there was a discontinuous surge that stopped just upstream of the LSPIV measurements before the first
238 measured surge passed through the reach. The first two measured surges were large enough to distinguish the front (S1 and
239 S2) and tail (S1 tail S2 tail) and the latter two were too small and were kept undivided (S3 and S4). There seemed to be a
240 higher water content with longer sustained fronts (compared to 2013). The S4 was unusually fast which behaved more of a
241 wave passing through the filled-up sediment trap of highly saturated deposit.

242 The 2015 event was especially interesting because of the [surges variable rheology](#). High-intensity rainfall covered the entire
243 catchment triggering many different source areas. The first surge (S1) had little sediment but carried a lot of large woody
244 debris. S2 was a slower muddier flow, however cobbles and boulders were also transported. S3 was a larger and even slower
245 muddy flow, carrying boulders, cobbles, and large woody debris. S4 is the slowest surge and a more visco-plastic flow still
246 carrying cobbles. S5 is similar to S4 but carried [fewer](#) cobbles. [In between these surges the low-flow material stops](#), the
247 visco-plastic material waited for the next surge to push it forward. A low steady muddy flow continued for another 30 min
248 with smaller surges. However, the sediment trap became filled creating a saturated pool of sediment making surges difficult
249 to pass through.

Deleted: From
Deleted: 2011-2015

Deleted:

Deleted: variation of surges
Deleted:

Deleted: less

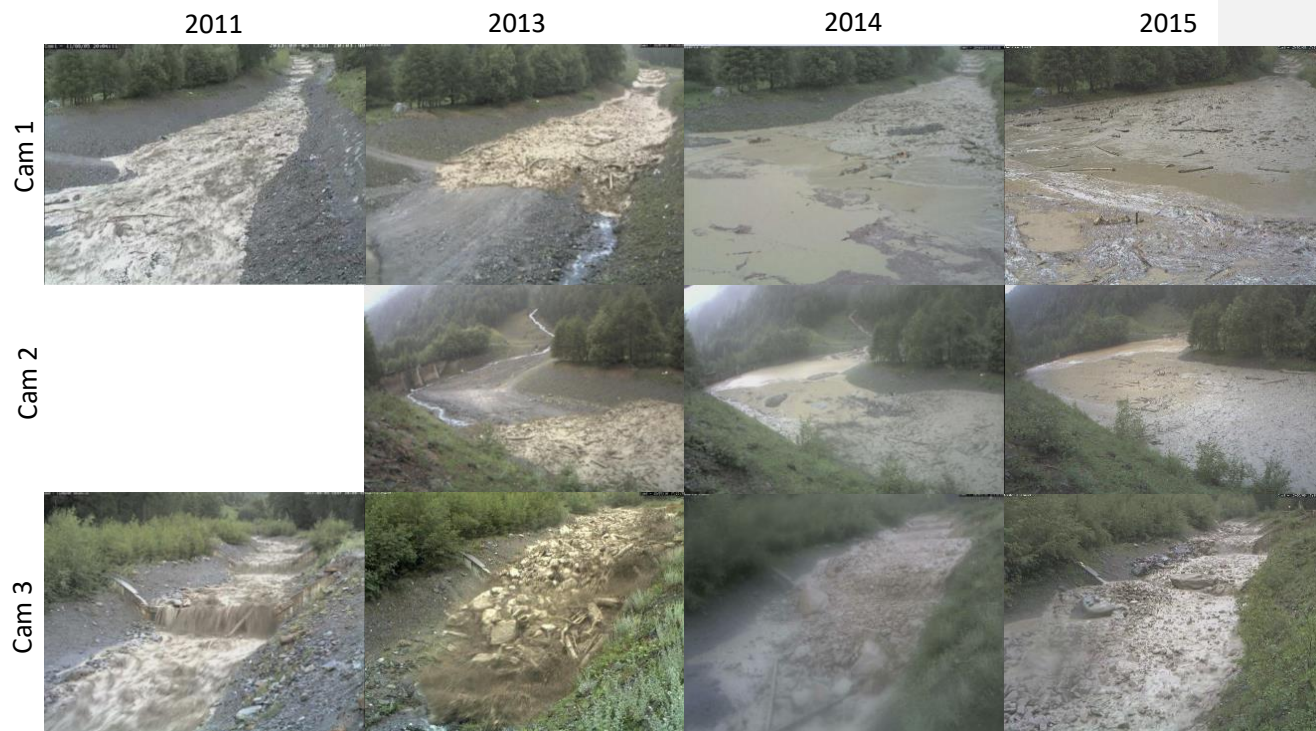


Figure 3: Views of the three cameras during the 2011, 2013, and 2014 debris flows. Cam 2 was selected for the LSPIV application due to the best positioning.

Table 2: Results of averaged LSPIV measurements, visual feature measurements on orthorectified images, and radar sensors (70 – 150 m upstream from the LSPIV section) for identifiable surges in 2011, 2013, 2014, 2015 (no events occurred in 2012).

| Event | Surge | Time | LSPIV | | | | Visual | | Radar Sensors (70 m and 150 m upstream from LSPIV) | |
|-------------|-----------|---------------------|----------------------------------|--------------|--------------------|-------------------------------|---------------------------|----------------------------------|--|-------------------|
| | | | velocity (m s ⁻¹) | width (m) | T_d (degrees) | T_r (m s ⁻¹) | sediment concentration | velocity (m s ⁻¹) | velocity (m s ⁻¹) | avg height (m) |
| 2011 | HF surge | 18:00 – 18:30 | -- | -- | -- | -- | low | -- | 2.6 | 0.6 |
| 2013 | S1 Front | 17:23:10 – 17:23:26 | <u>4.4</u> | <u>19</u> | <u>24.5</u> | <u>2.7</u> | high | 4.4 | 5.7 | 1.9 |
| | S1 Inter. | 17:23:35 – 17:23:42 | <u>3.1</u> | <u>18</u> | <u>15.2</u> | <u>1.3</u> | medium | 2.4 | -- | 1.6 |
| | S1 Tail | 17:23:43 – 17:24:05 | <u>1.9</u> | <u>17</u> | <u>24.6</u> | <u>1.3</u> | medium | 2.6 | -- | 1.0 |
| 2014 | Pre-surge | 17:13:45 – 17:15:13 | <u>3.2</u> | <u>7</u> | <u>33.8</u> | <u>2.2</u> | low | 2.7 | -- | 0.4 |
| | S1* | 17:22:01 – 17:22:17 | <u>4.6</u> | <u>23</u> | <u>36.0</u> | <u>2.8</u> | medium | 5.6 | 5.3 | 1 |
| | S1 tail* | 17:22:20 – 17:22:49 | <u>4.2</u> | <u>13</u> | <u>32.6</u> | <u>3.1</u> | medium | 4.4 | 4.8 | 0.5 |
| | S2 | 17:25:43 – 17:26:04 | <u>3.1</u> | <u>22</u> | <u>32.3</u> | <u>2.8</u> | high | 3.3 | 4.1 | 0.9 |
| | S2 tail | 17:26:10 – 17:27:00 | <u>2.9</u> | <u>15</u> | <u>34.1</u> | <u>2.6</u> | high | 2.8 | 3.6 | 0.7 |
| | S3 | 17:29:24 – 17:29:40 | <u>3.9</u> | <u>14</u> | <u>32.3</u> | <u>3.3</u> | high | 4.4 | 4.8 | 0.9 |
| | S4 (wave) | 17:30:13 – 17:30:21 | <u>6.2</u> | <u>8</u> | <u>31.3</u> | <u>4.2</u> | low | 6.9 | 3.5 | 0.7 |
| | | | | | | | | | | |
| 2015 | S1 | 17:16:52 – 17:17:15 | <u>5.6</u> | <u>14</u> | <u>33.2</u> | <u>3.0</u> | low | 4.9 | -- | 0.8 |
| | S2 | 17:20:05 – 17:21:02 | <u>2.5</u> | <u>17</u> | <u>30.7</u> | <u>2.8</u> | high | 3.0 | 3.5 | 0.8 |
| | S3 | 17:23:30 – 17:24:01 | <u>2.2</u> | <u>22</u> | <u>29.2</u> | <u>2.5</u> | high | 1.5 | 3.5 | 1.25 |
| | S4 | 17:24:25 – 17:25:12 | <u>0.6</u> | <u>20</u> | <u>21.5</u> | <u>1.1</u> | very high | 0.7 | -- | 0.6 |
| | S5 | 17:26:54 – 17:27:39 | <u>0.8</u> | <u>16</u> | <u>9.4</u> | <u>0.6</u> | very high | 1.0 | -- | 0.8 |

* the first actual debris flow surge stopped between the LSPIV and the radar, it remobilized with S1.

267 **5 Results**

268 **5.1 Surface flow velocities**

269 LSPIV results of the three analysed debris flows were extracted from the upstream cross-section of the LSPIV reach (XS in
270 Fig. 1C). This makes surge comparisons more accurate because it is located in a more stable and confined location, rather
271 than the open sediment trap that fills up during the events. Mean surge velocities ranged from 0.6 to 6.2 m/s, velocity
272 variation turbulence (T_v) from 0.6 to 4.2 m/s, and directional variation turbulence (T_d) from 9.4 to 36.0 degrees (Table 2; Fig.
273 4). The instantaneous velocities for the 2013 event have smaller variations compared to the other events. The minimum
274 recording frequency was 3 fps for 2013 rather than 2 fps for 2014 and 2015 because of the available light during the storms.
275 The highest velocity (2014 S4) had a significantly higher T_v , which is expected for a wave passing through a slurry.
276 The LSPIV velocities seem fairly accurate considering the low camera frequency (2-3 fps), camera angle, 5 cm/pixel
277 resolution and the unsteadiness of the flows. Their average velocities at a given cross-section were compared with manual
278 measurements of identifiable features on the same orthorectified images (feature picking) to validate the LSPIV cross-
279 correlation matching (Table 2; Fig. 5). The LSPIV has a slight under estimation with a mean difference of -0.1 m/s and a
280 standard deviation of 0.54 m/s. The LSPIV estimates are however more robust because of the large sample sizes and the
281 feature picking does not always represent the flow velocity accurately.
282 The LSPIV velocities are also compared with the velocities measured by the radar sensors 70 - 150 m upstream (located in
283 Fig. 1). Given the downstream decrease in velocity, the agreement is satisfactory with a mean difference of -0.9 m/s and a
284 standard deviation of 0.25 m/s (Table 2; Fig. 5). Not all of the surges could be traced from the radar sensors to the LSPIV
285 reach, rather they will stop and be pushed by the next surge. This is especially the case with the visco-plastic surges in 2015.

- Deleted: and mean horizontal
- Deleted: ,
- Deleted: 14.5
- Deleted: 35.
- Deleted: 2
- Deleted: degrees
- Deleted: en
- Deleted: the largest variation indicating the degrading accuracy

- Deleted: from
- Deleted: Given the downstream decrease in velocity, the velocities are also aggregable

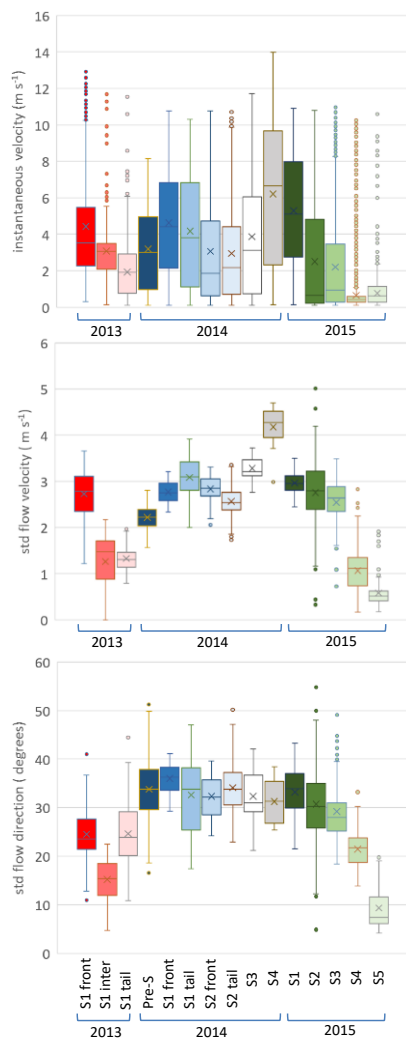


Figure 4: LSPIV velocity (top), velocity variation (T_v) (middle), and directional variation (T_d) (bottom) comparisons for 2013, 2014, 2015 surges located at the same cross-section.

Deleted: and

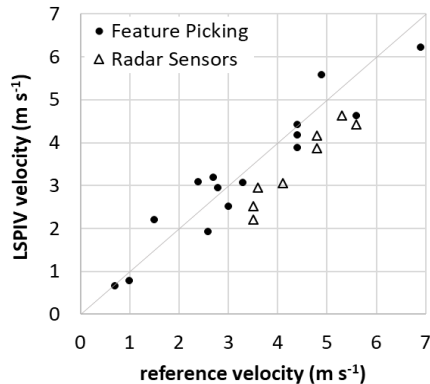


Figure 5: LSPIV velocities compared with velocities derived from feature picking in the orthorectified image sequences and radar sensors located 70 – 150 m upstream.

5.2 Pattern of flow velocities from the 2013 debris flow

The LSPIV results can be presented and analyzed in several different ways. For the 2013 debris flow, we show the map view of the average velocities for the front (17:23:10 - 17:23:26), intermediate (17:23:35 - 17:23:42) and tail (17:23:43 - 17:24:05) (Fig. 6). Despite the simple shape of the 2013 debris flow hydrograph (Comiti et al., 2014), it had a very interesting dynamic when entering the sediment trap. The front has high scattered average velocities covering the whole reach. The intermediate (transition from front to tail) shows a distinct decrease in velocity with a more homogeneous distribution. Zero velocities correspond with the boulder front deposition. The low-velocity tail becomes more confined traveling around the boulder front as a more laminar flow (Fig. 6C).

Three cross-sections were examined to compare the velocity-time profiles of the event (Fig. 7b). The peak velocity in the front gradually decreases in duration, nonetheless when traveling through the reach the velocity remains relatively high. For the intermediate part, there is a distinct slump in velocity where the boulder front was deposited in cross section X2. The tail of the debris flow increases downstream, this is expected since the boulders confined the channel. In Figure 7a, the LSPIV computation domain is overlapped on a map of the residual height, computed on the pre-event topography as the cell-by-cell difference between the SfM DEM and a smoothed mean DEM, whose cells have a value equal to the mean of the neighboring cells at a 5-m scale (Cavalli and Marchi, 2008). The residual height shows the general form of the channel revealing the smaller confined channel along the left bank and larger convex features covering the center and right bank.

Deleted: ¶
The LSPIV study was fixed within one reach which limited our perspective in the spatial distribution of the surge velocities. Therefore we took advantage of the three monitoring cameras to generally estimate the propagation of the flow over a span of 250 m. The visual estimates of observable debris flow fronts show a large variation of slope-velocity trends (Fig. 6). Most of the surges are clearly dependent on slope. However, some surges (2014 S2,S3; 2015 S1, S3) have no apparent dependence on slope because of disruptions to the flow such as log jams and very visco-plastic flows. Longer multiple reaches of LSPIV studies will be needed to better understand the continuity of the surges and their relationship between turbulence and slope.¶

Figure 6: Front velocities (estimated from observable fronts passing by distinct features in Cam 1, 2, and 3) are plotted according to distance from the end of the sediment trap (left) and local slope (right).¶

- Deleted:** 7
- Deleted:** Despite the classic form of the 2013 debris flow
- Deleted:**
- Deleted:** 8
- Deleted:** 8
- Deleted:** B
- Deleted:** 8
- Deleted:** et al.
- Deleted:** (Fig. 8)

351 These features correspond with the flow dynamics seen in Figure 7, with the boulder front depositing on the higher convex
352 features with the water surge passing around in the lower confined channel.

353 The longitudinal profile of the average velocities combined with the video imagery and multi-date topography (Fig. 8)
354 distinctly show the boulder front depositing after the sudden decrease in local slope (down to a negative slope) and channel
355 widening. The front average velocity remains constant even after the deposition of boulders. The intermediate part of the
356 surge shows the correspondence of the decreased velocity and the deposition. The boulder deposit narrows the channel and
357 therefore increases the velocity for the tail of the flow. The tail has an unusual increase of velocity at the downstream end
358 despite the local widening of the channel with decreasing velocity. Either there was a released plugging upstream or there
359 was an important decrease of sediment concentration (upstream deposition).

360 Several studies observe peak velocities of debris flows located behind the boulder front (Pierson, 1986; Arattano and Marchi,
361 2000; Suwa, 1993). The high concentration of the interlocking boulders creates a high frictional resistance and low mobility
362 (Pierson, 1986; Suwa, 1993). Debris flow channels typically have several reaches with important narrowing and widening
363 and naturally the velocity longitudinal profile must adjust to each channel reach. When the front is confined, boulders
364 interlock, velocities are higher behind the front as previous studies showed. In our case, we observe the boulders unlocking
365 which creates more mobility where the peak velocity is in the very front of the flow. The boulders laterally deposit as a levee
366 because of the decrease in transport capacity.

Deleted: 8

Deleted: 9

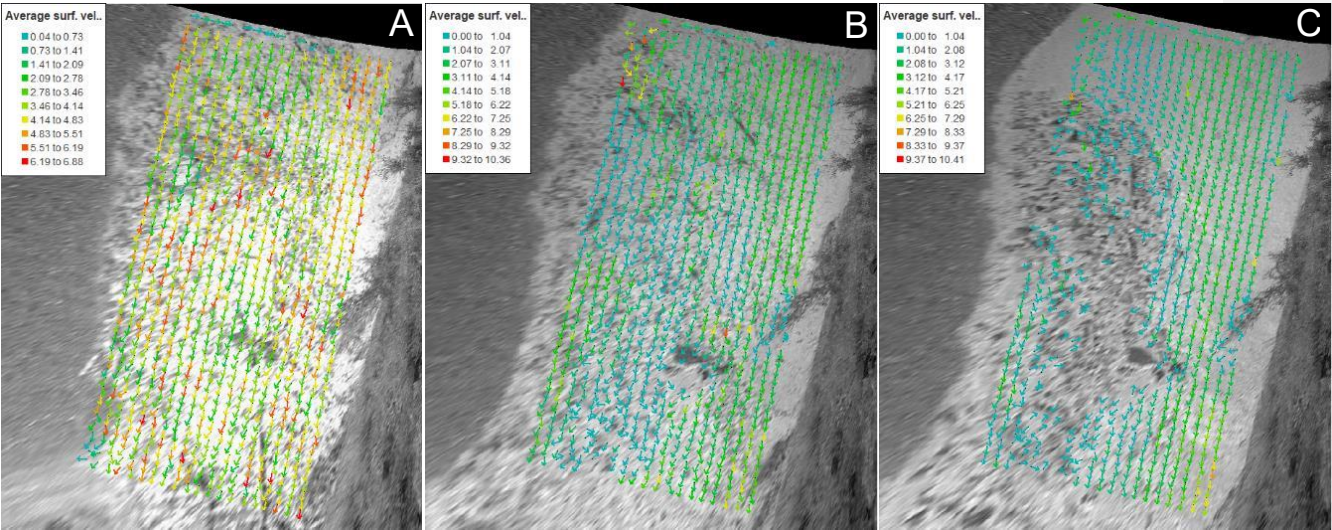


Figure 6: Average LSPIV velocities (m s⁻¹) for the 2013 debris flow front (A) intermediate (B) and tail (C).

Deleted: 7

Deleted:

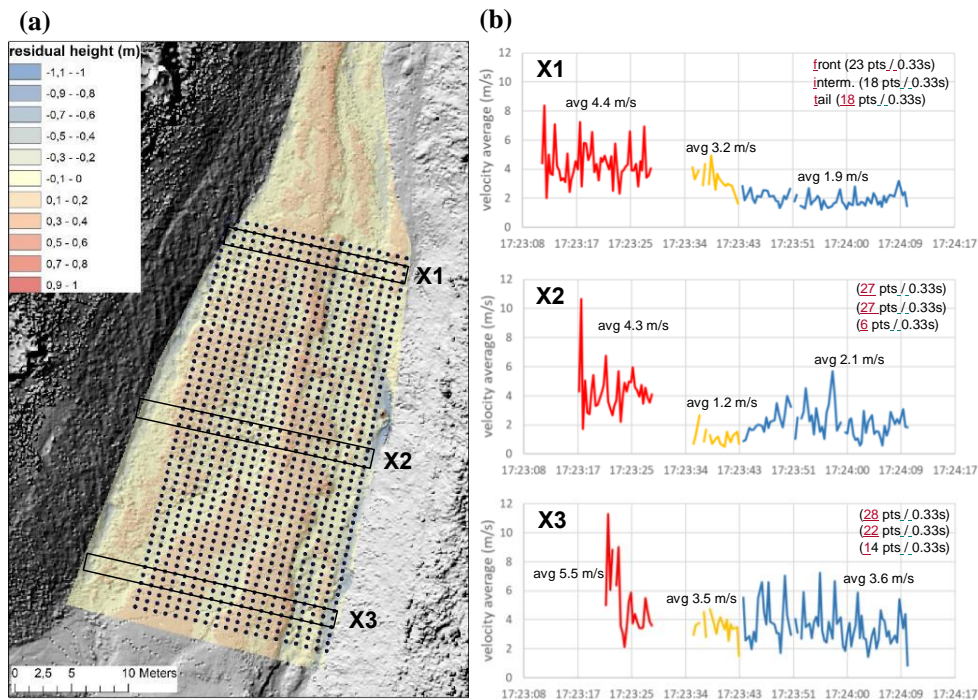


Figure 7: (a) Preliminary residual elevation of the channel bed at a 5-m scale, the grid of LSPIV calculations is shown with cross-section X1-3 outlined; (b) 2013 debris-flow LSPIV velocity time series (3 fps) at three cross-sections (X1, X2, and X3) with red (front), yellow (intermediate), and blue (tail). The velocity variation mostly represents the turbulence; however, some noise can come from low point density. The time interruption between the front and intermediate was initially made in the LSPIV analysis to clearly distinguish the two.

Deleted: 8

Deleted: A

Deleted: B

Deleted: C

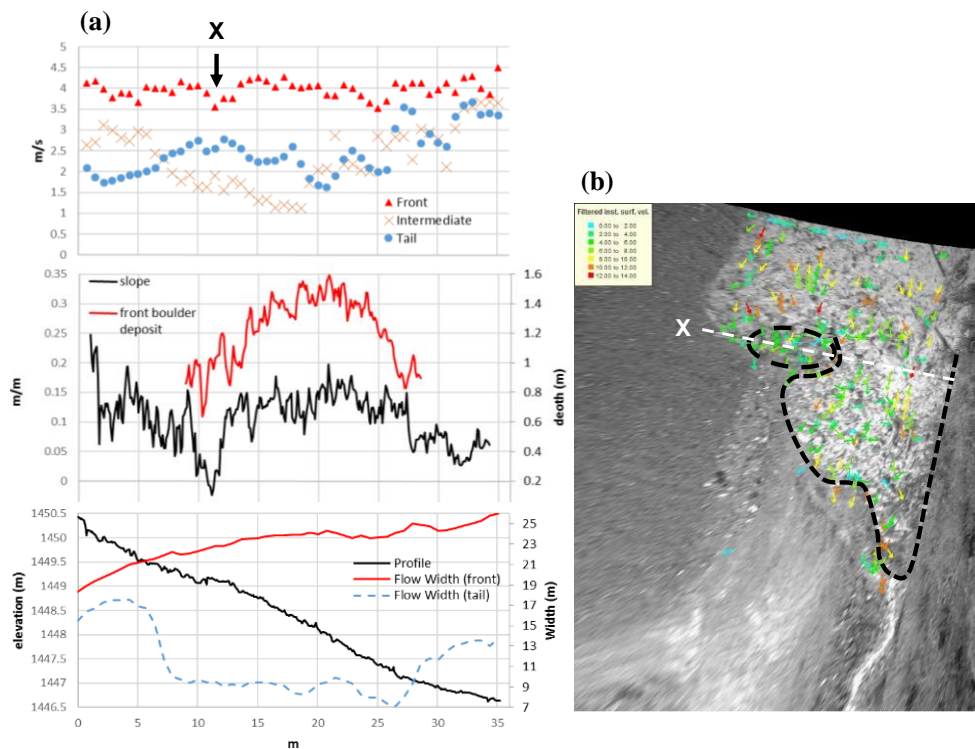


Figure 8: (a) The 2013 debris flow LSPIV average velocity of the front (red), intermediate (yellow), and tail (blue) traveling downstream (along the long profile of the grid in Figure 7). Local slope and the boulder front deposit (from multi-date SfM) are also plotted along the distance (center) as well as pre-event elevation and flow width of both the front and tail (bottom). At cross-section X, the boulder front is seen to deposit while the watery surge passes around it (b) which gives constant peak velocity in the front of the surge (despite the front deposition).

Deleted: 9

Deleted: (top)

Deleted: seen on the right image

396 5.3 Horizontal turbulence index

397 Sediment concentration, viscosity, and yield strength are rheological parameters that can influence the turbulence and are
398 commonly associated with flow resistance coefficients (eg. Rickenmann and Recking, 2011). For all the surges in 2013-
399 2015, we found that turbulence has a strong relation with the surge velocity (Fig. 9), whereas flow heights and flow widths
400 had much lower correlation with surge velocities. We compared both directional turbulence (T_d) and velocity turbulence (T_v)
401 index measurements (see section 3.3) to the empirical flow resistance equation for debris flows from Koch et al. (1998),
402 described in Rickenmann (1999):

403
$$C = \frac{V}{H^{0.3} S^{0.5}}, \quad (1)$$

404 where velocity (V) is the average LSPIV velocity for each surge, slope (S) being constant, flow height (H) measured
405 upstream from the radar sensors (thereby introducing an additional source of error), and the flow resistance coefficient (C).
406 The T_v clearly has a stronger correlation than the T_d when compared with V and C (Fig. 9). Based on the data analyzed, the
407 power-law equation that links T_v to the flow velocity V through the coefficient C is:

408
$$V = 3.91 T_v^{1.06} H^{0.3} S^{0.5},$$

410 however, more surges need to be measured to better define the function. The influence of spatial and temporal sampling
411 resolutions also needs to be better understood for further application.

412 Sediment concentrations from visual estimates (Table 2) were used to classify these comparisons which shows a better
413 correspondence with T_v than T_d when comparing with C for the debris flow fronts. Sediment concentrations for the tails or
414 waves did not correspond well, probably because of influences of fluid pressures from the front and the pooling of slurry in
415 the sediment trap. Visual estimates of sediment concentrations become difficult to classify, especially in higher turbulence,
416 however there still remains to be a strong relationship between T_d and C .

417 For some of the surges, boulders and logs can be seen rotating, resulting in misrepresentative flow directions and velocity
418 fluctuations. Our interrogation area (1.3 m) for LSPIV calculations was aimed to characterize the general flow characteristics
419 where these misrepresentations are either too detailed or have little influence on the high sampling of the LSPIV method.
420 Higher image resolution and camera speed might give further insight on boulder dynamics and log jamming.
421

- Deleted: et al.,
- Deleted: 1999
- Deleted: 10
- Deleted: whereas flow heights and flow widths had little influence on the surge velocities
- Deleted: our horizontal
- Deleted: (T_h)
- Deleted: an empirical review from
- Deleted: et al.

- Deleted: strongly correlates with the variation of
- Deleted: mean surge velocities
- Deleted: 10
- Deleted: We begin to see suspect that T_v has a relationship with the coefficient by using a power-law with the velocity function written as:
- Deleted: $V = 3.909 T_v^{1.0603} H^{0.3} S^{0.5}, (2)$
- Formatted: Highlight

- Deleted: Laminar and turbulent flows are often defined according to Froude's critical number.¶
 $F = \frac{V}{\sqrt{gH}} = 1, \dots \dots \dots (3)$ ¶
where below 1 is laminar and above 1 is turbulent (Enos, 1977). Froude's function (F) was compared with T_h showing similar trends as with C (Fig. 9).
- Deleted: is
- Deleted: showing
- Deleted: good
- Deleted: versus
- Deleted: F
- Deleted: around the critical Froude's number
- Deleted: F (Fig. 10) written as:¶
 $V = 0.0005 T_h^{2.2823} \sqrt{gH}, \dots \dots \dots (4)$

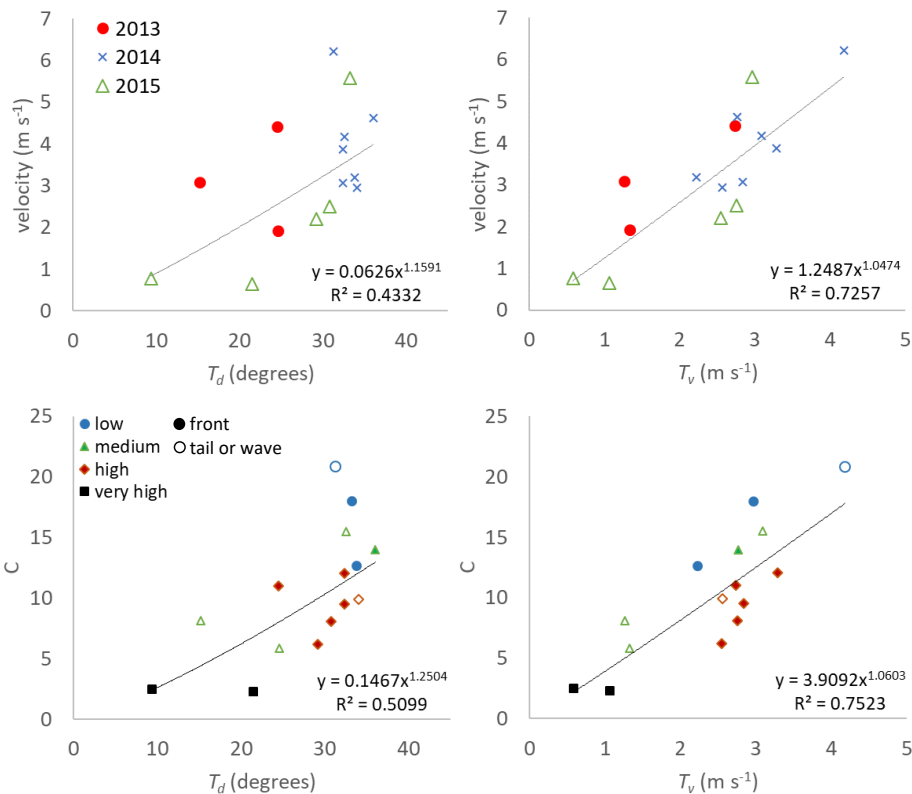


Figure 9: Classified by events (top), the directional turbulence index (T_d) (left) and velocity turbulence index (T_v) (right) are compared to LSPIV average surge velocity (top). Classified by visually estimated sediment concentrations (bottom) from Table 2, the T_d and T_v are compared to the flow resistance coefficient (C) (Eq. 1).

Deleted: 10

Deleted: horizontal

Formatted: Font: Italic

Deleted: Classified by visually estimated sediment concentrations from Table 2 (bottom), the T_d compared to LSPIV average surge velocity (left) and Froude's number (Eq. 3) (right). The highest velocity and coefficient is an outlier influenced by impact or rolling wave since it was the last surge of the event traveling through the filled fully saturated sediment trap.

465 6 Conclusions

466 We have presented LSPIV-derived velocities for three debris flow events in the Gatria channel, for a total of 11 surges and
467 these velocities were compared with manual measurements on the ortho-rectified imagery (mean difference of -0.1 m s^{-1})
468 and upstream radar sensors (mean difference of -0.9 m s^{-1}). LSPIV appears to be a reliable method for measuring velocities
469 of such flows, and to the best of our knowledge, this is one of the first studies on the topic. The variation of vectors from the
470 LSPIV was introduced as an index of horizontal turbulence according to directional variation (T_d) and velocity variation (T_v).

471 Within the studied reach, debris flows varied in velocity and turbulence among different events, among individual surges
472 within an event, and even within each surge. Several contributing factors can explain the variation such as rainfall
473 variability, activation of variable source areas, channel storage levels, check-dam failures, boulder and log jamming, and just
474 the complex interactions between the channel dynamic and the flow. For example, the 2015 event distinctly had the largest
475 variation of surge velocities and turbulence that most likely caused by the burst of rainfall distributed over most of the
476 catchment, which in turn activated more source areas than other events. The 2013 debris flow showed that a gentle relief in
477 the channel opening can influence the front material deposition but not decrease the mean front velocity because of the water
478 surge passing through and around the unlocking boulders. A strong power-law relationship is found between velocity and
479 the T_v as well as the flow resistance coefficient C in the empirical equation of Koch et al. (1998). We propose that the T_v
480 measurement improves the flow resistance coefficient for estimating velocity and T_d gives a better representation of sediment
481 concentration.

482 LSPIV application on debris flows has shown to be very effective but there still needs to be a better understanding of the
483 spatial and time resolution and the influence of slope. Some suggestions can be made for this type of monitoring, such as 1)
484 be sure that the minimum frame rate of the IP camera is high enough to capture the movement (≤ 2 fps, depending on the
485 flow velocity) or use a fixed frame rate from an analog camera; 2) locate the cameras to a stable reach with high viewing
486 positions that are perpendicular to the flow; and 3) overlap the study area directly over stage sensors for discharge
487 measurements for proper analysis of turbulence. Further studies can also involve calibrating geophones with the turbulence
488 measurements which are more easily distributed in the field.

489 Further research on LSPIV derived velocity and turbulence needs to address the influence of confinement and roughness of
490 the channel bed. Debris-flow channels have intermediate and large-scale roughness that make flow velocities and turbulence
491 more variable as flow heights decrease (Rickenmann and Recking, 2011; Ferguson, 2012). Large-scale roughness can effect
492 the confinement of the channel such as a large boulder or a debris-flow levee. Pre-event high-resolution elevation models
493 and their residual heights and standard deviations at varying scales (Cavalli and Marchi, 2008) will provide better insight on
494 spatial distribution of debris-flow velocities when they are directly compared with LSPIV measurements.

Deleted: type of

Deleted: geophysical

Deleted: directional

Deleted: between

Deleted: between

Deleted: Visual estimates of front velocities were also made from three monitoring cameras to quantify the spatial distribution showing various slope-velocity trends. Higher sediment concentrated and visco-plastic surges tend to stop in the channel and wait for the push of the next surge. This shows the discontinuity of the debris flow propagation that holds in question in how we can infer these observations upstream and downstream.

Deleted: The

Deleted: T_h

Deleted: Th

Deleted:

Deleted:

Deleted:

Deleted: et al.

Deleted: u

515 **Acknowledgements**

516 Funding for this research came from the research project “Kinoflow” funded by the Autonomous Province of Bozen-
517 Bolzano. The debris-flow monitoring station of Gadoria catchment is managed by the Civil Protection Agency of the
518 Autonomous Province of Bozen-Bolzano. A preliminary analysis of the debris-flow hydrograph conducted by V.
519 D’Agostino and F. Bettella (Department TeSAF, University of Padova) helped interpret the 2014 event. We also thank
520 Alexandre Hauet (EDF-DTG Grenoble) who provided guidance and advice for the Fudaa-LSPIV application.

521 **References**

522 Aigner J., Habersack H., Rindler R., Blamauer B., Wagner B., Schober B., Comiti F., Dell’Agnese A., Engel M., Liébault F.,
523 Bel C., Bellot H., Fontaine F., Piegay H., Benacchio V., Lemaire P., Ruiz-Villanueva V., Vaudor L., Cavalli M., Marchi L.,
524 Crema S., Brardinoni, F., Bezak N., Rusjan S., Mikoš M., Abel J., Becht M., Heckmann T., Rimböck A., Schwaller G.,
525 Höhne R., Cesca M., Vianello A., Krivograd Klemenčič A., Papež J., Lenzi M.A., Picco L., Moretto J., Ravazzolo D., Jäger
526 G., Moser M., Hübl J., and Chiari M.: Sed ALP – Sediment Management in Alpine Basins (www.sedalp.eu), WP5 Report -
527 Sediment transport monitoring, 256 p., 2015.

528 Arattano, M. and Grattoni, P.: Using a fixed video camera to measure debris-flow surface velocity. Proceedings of the
529 Second International Conference on Debris-flow Hazards Mitigation: Mechanics, Prediction, and Assessment, Taipei, 16-18
530 August, 2000; Wiecezorek, G., Naeser, N., Eds.; A.A. Balkema: Rotterdam, 2000; 273–281, 2000.

531 Arattano, M. and Marchi, L.: Video-derived velocity distribution along a debris flow surge, Physics and Chemistry of the
532 Earth: Part B 25 (8), 781-784, 2000.

533 Arattano, M., Marchi, L., and Cavalli, M.: Analysis of debris-flow recordings in an instrumented basin: confirmations and
534 new findings, Natural Hazards and Earth System Science, 12(3), 679-686, 2012.

535 Berti, M.R., Genevois, R., LaHusen, R.G., Simoni, A., and Tecca, P.R.: Debris flow monitoring in the Acquabona watershed
536 in the Dolomites (Italian Alps), Phys. Chem. Earth, Part B, 25(9), 707-715, 2000.

537 Cavalli M., and Marchi L.: Characterisation of the surface morphology of an alpine alluvial fan using airborne LiDAR.
538 Natural Hazards and Earth System Sciences, 8 (2), 323-333, 2008.

539 Cavalli, M., Trevisani, S., Comiti, F., and Marchi, L.: Geomorphometric assessment of spatial sediment connectivity in small
540 Alpine catchments, Geomorphology, 188, 31-41, doi:10.1016/j.geomorph.2012.05.007, 2013.

541 Cavalli, M., Goldin, B., Comiti, F., Brardinoni, F., and Marchi, L.: Assessment of erosion and deposition in steep mountain
542 basins by differencing sequential digital terrain models, Geomorphology, 291, 4-16, doi:10.1016/j.geomorph.2016.04.009,
543 2017.

544 Chen, C.L.: Comprehensive review of debris flow modeling concepts in Japan, In: J.E. Costa, G.F. Wiecezorek (Eds.),
545 Reviews in engineering geology, vol VII. Debris flows/ avalanches: process, recognition, and mitigation., Boulder, CO, 13-
546 29, 1987.

Deleted: Arattano, M., Marchi, L., and Cavalli, M.: Analysis of debris-flow recordings in an instrumented basin: confirmations and new findings. Natural Hazards and Earth System Science, 12(3), 679-686, 2012.¶

Deleted: Arattano, M., Bertoldi, G., Cavalli, M., Comiti, F., D’Agostino, V., and Theule, J.: Comparison of Methods and Procedures for Debris-Flow Volume Estimation, Engineering Geology for Society and Territory - Volume 3, 115-119, 2015.¶

Formatted: Do not check spelling or grammar

Deleted: Cavalli, M., Tarolli, P., Marchi, L., and Dalla Fontana, G.: The effectiveness of airborne LiDAR data in the recognition of channel-bed morphology, Catena, 73(3), 249-260, 2008.¶

Deleted: .

Deleted: :

Deleted: 6

561 [Coe J.A., Kinner D.A., Godt J.W.: Initiation conditions for debris flows generated by runoff at Chalk Cliffs, central](#)
562 [Colorado, Geomorphology, 96, 270–297, 2008.](#)

563 Comiti F., Marchi L., Macconi P., Arattano M., Bertoldi G., Borga M., Brardinoni F., Cavalli M., D’Agostino V., Penna D.,
564 and Theule J.: A new monitoring station for debris flows in the European Alps: first observations in the Gadria basin, Nat
565 Hazards 73:1175–1198. doi:10.1007/s11069-014-1088-5, 2014.

566 Costa, J.E.: Physical geomorphology of debris flows. In: J.E. Costa, P.J. Fleisher (Eds.), Developments and Applications in
567 Geomorphology, Springer Verlag, 268-317, 1984.

568 D’Agostino, V. and Bertoldi, G.: On the assessment of the management priority of sediment source areas in a debris-flow
569 catchment, Earth Surface Processes and Landforms, 39 (5), 656-668, DOI: 10.1002/esp.3518, 2014.

570 [Ferguson, R. I.: River channel slope, flow resistance, and gravel entrainment thresholds, Water Resources Research 48:](#)
571 [W05517. DOI: 10.1029/2011WR010850, 2012.](#)

572 Fujita, I., M. Muste, and A. Kruger: Large-scale particle image velocimetry for flow analysis in hydraulic engineering
573 applications, J. Hydraul. Res., 36(3), 397–414, 1998.

574 Genevois, A., [Galgaro, R.](#), and Tecca, P.R.: Image analysis for debris flow properties estimation, Physics and Chemistry of
575 the Earth, Part C 26, 623–631, 2001.

576 Hauet A., Creutin J.-D., and Belleudy P.: Sensitivity study of large-scale particle image velocimetry measurement of river
577 discharge using numerical simulation, Journal of Hydrology 349(1–2): 178–190, 2008.

578 Hungr, O., Evans, S.G., Bovis, M., and Hutchinson, J.N.: Review of classification of landslides of flow type, Environmental
579 and Engineering Geoscience, VII, 221-238, 2001.

580 Hungr, O., Morgan, G.C., and Kellerhals, R.: Quantitative analysis of debris torrent hazards for design of remedial measures,
581 Canadian Geotechnical Journal, 21, 663-677, 1984.

582 Hürlimann, M., Rickenmann, D., and Graf, C.: Field and monitoring data of debris-flow events in the Swiss Alps, Canadian
583 Geotechnical Journal, 40(1), 161-175, 2003.

584 Iverson, R.M.: The physics of debris flows. Reviews of Geophysics, 35(3), 245-296, 1997.

585 [Jacquemart, M., Meier, L., Graf, C., and Morsdorf, M.: 3D dynamics of debris flows quantified at sub-second intervals from](#)
586 [laser profiles, Nat Hazards 89:785. doi.org/10.1007/s11069-017-2993-1.](#)

587 Javernick L., Brasington J., and Caruso B.: Modelling the topography of shallow braided rivers using structure-from-motion
588 photogrammetry, Geomorphology 213: 166–182, 2014.

589 Koch, T.: Testing various constitutive equations for debris flow modelling. In: K.e.a. Kovar (Ed.), Hydrology, Water
590 Resources and Ecology in Headwaters, IAHS, Publ. No. 248, Merano, Italy, 249-257, 1998.

591 Le Boursicaud, R., Pénard, L., Hauet, A., Thollet, F., and Le Coz, J.: Gauging extreme floods on YouTube: application of
592 LSPIV to home movies for the post-event determination of stream discharges, Hydrol. Process. 30, 90–105, 2016.

593 Le Coz, J., Hauet A., Pierrefeu G., Dramais G., and Camenen B.: Performance of image-based velocimetry (LSPIV) applied
594 to flashflood discharge measurements in Mediterranean rivers, J. Hydrol., 394(1), 42–52, 2010.

Deleted: Enos, P.: Flow regimes in debris flow. Sedimentology 24, 1, 133–142, 1977.¶

Deleted: Calgaro

Formatted: English (United States)

598 Le Coz J., Jodeau M., Hauet A., Marchand B., and Le Boursicaud R.: Image-based velocity and discharge measurements in
 599 field and laboratory river engineering studies using the free Fudaa-LSPIV software, *Proceedings of the International*
 600 *Conference on Fluvial Hydraulics, RIVER FLOW 2014*, 1961–1967, 2014.
 601 Marchi, L., Arattano, M., and Deganutti, A.M.: Ten years of debris-flow monitoring in the Moscardo Torrent (Italian Alps),
 602 *Geomorphology*, 46, 1-17, 2002.
 603 McCoy, S.W., Kean, J.W., Coe, J.A., Staley, D.M., Wasklewicz, T.A., and Tucker, G.E.: Evolution of a natural debris flow:
 604 in situ measurements of flow dynamics, video imagery, and terrestrial laser scanning, *Geology*, 38(8), 735-738, 2010.
 605 Muste, M., Hauet A., Fujita I., Legout C., and Ho H.-C.: Capabilities of large-scale particle image velocimetry to
 606 characterize shallow free-surface flows, *Adv. Water Resour.*, 70(0), 160–171, doi:10.1016/j.advwatres.2014.04.004, 2014.
 607 Navratil, O., Liébault, F., Bellot, H., Travaglini, E., Theule, J., Chambon, G., and Laigle, D.: High-frequency monitoring of
 608 debris-flow propagation along the Réal Torrent, Southern French Prealps, *Geomorphology* 201, 157–171, 2013.
 609 Phillips, C.J. and Davies, T.R.H.: Determining rheological parameters of debris flow material, *Geomorphology*, 4, 101-110,
 610 1991.
 611 Piermattei, L., Carturan, L., and Guarnieri, A.: Use of terrestrial photogrammetry based on structure-from-motion for mass
 612 balance estimation of a small glacier in the Italian alps, *Earth Surf. Proc. Land.*, 40, 1791–1802, doi:10.1002/esp.3756, 2015.
 613 Pierson, T.C.: Flow behavior of channelized debris flows, Mt. St. Helens, Washington, *Hillslope Processes*. Allen & Unwin,
 614 Boston, 1986.
 615 Pierson, T.C. and Scott, K.M.: Downstream Dilution of a Lahar: Transition from Debris Flow to Hyperconcentrated
 616 Streamflow, *Water Resources Research*, 21(10), 1511-1524, 1985.
 617 Prochaska, A.B., Santi, P.M., Higgins, J.D., and Cannon, S.H.: A study of methods to estimate debris flow velocity,
 618 *Landslides*, DOI 10.1007/s10346-008-0137-0, 2008.
 619 Rickenmann, D.: Empirical relationships for debris flows, *Natural Hazards*, 19(1), 47-77, 1999.
 620 Rickenmann, D. and Recking, A.: Evaluation of flow resistance in gravel-bed rivers through a large field data set, *Water*
 621 *Resources Research* 47: W07538. DOI: 10.1029/2010wr009793, 2011.
 622 Rickenmann, D., Weber, D., and Stepanov, B.: Erosion by debris flows in field and laboratory experiments. In: D.
 623 Rickenmann, C.L. Chen (Eds.), *Debris-Flow Hazards Mitigation: Mechanics, Prediction, and Assessment*. Millpress,
 624 Rotterdam, The Netherlands, 883-894, 2003.
 625 Scheidl, C., McArdell, B.W., and Rickenmann, D.: Debris-flow velocities and superelevation in a curved laboratory channel,
 626 *Can. Geotech. J.* 52, 305–317, doi: 10.1139/cgj-2014-0081, 2014.
 627 Stumpf, A., Augereau E., Delacourt C., and Bonnier J.: Photogrammetric discharge monitoring of small tropical mountain
 628 rivers: A case study at Rivière des Pluies, Réunion Island, *Water Resour. Res.*, 52, doi:10.1002/2015WR018292, 2016.
 629 Suwa, H., Okunishi, K., and Sakai, M.: Motion, debris size and scale of debris flows in a valley on Mount Yakedake, Japan,
 630 *IAHS Publ. No. 217*, 239–248, 1993.

631 Westoby, M. J., Brasington, J., Glasser, N. F., Hambrey, M. J., and Reynolds, J. M.: “Structure-from-Motion”
632 photogrammetry: A low-cost, effective tool for geoscience applications, *Geomorphology*, 179, 300–314,
633 doi:10.1016/j.geomorph.2012.08.021, 2012.

634